

## RESEARCH ARTICLE

### Dislocation dynamics simulations with climb: kinetics of dislocation loop coarsening controlled by bulk diffusion

Botond Bakó<sup>a</sup>, Emmanuel Clouet<sup>a\*</sup>, Laurent M. Dupuy<sup>b</sup> and Marc Blétry<sup>c</sup>

<sup>a</sup> *CEA, DEN, Service de Recherches de Métallurgie Physique,  
91191 Gif-sur-Yvette, France*

<sup>b</sup> *CEA, DEN, Service de Recherches de Métallurgie Appliquée,  
91191 Gif-sur-Yvette, France*

<sup>c</sup> *Institut de Chimie et des Matériaux Paris-Est, CNRS UMR 7182,  
2-8, rue Henri Dunant, 94320 Thiais, France*

(Received 00 Month 200x; final version received 00 Month 200x)

Dislocation climb mobilities, assuming vacancy bulk diffusion, are derived and implemented in dislocation dynamics simulations to study the coarsening of vacancy prismatic loops in fcc metals. When loops cannot glide, the comparison of the simulations with a coarsening model based on the line tension approximation shows a good agreement. Dislocation dynamics simulations with both glide and climb are then performed. Allowing for glide of the loops along their prismatic cylinders leads to faster coarsening kinetics, as direct coalescence of the loops is now possible.

**Keywords:** dislocation climb; dislocation loops; coarsening; diffusion; dislocation dynamics

#### 1. Introduction

The strength of crystalline materials is mainly determined by the motion of dislocations, the carriers of plastic flow. At high temperatures the mechanical properties of metals and alloys can change fundamentally because of dislocation climb. Climb occurs when the motion of the dislocations has a component perpendicular to their glide plane. This requires the emission or absorption of point defects and their long-range diffusion. Due to the ability to annihilate edge dislocation dipoles, climb plays a fundamental role, for instance, in high temperature creep [1, 2] and recovery [3]. Climb mobility has also an important effect on dislocation morphology [4, 5]. Specifically, climb and cross-slip control the length scale of the cells of the dislocation network [6–8], and the suppression of climb leads to the freezing of the network into a diffuse-looking random distribution [8, 9]. It is thus highly desirable to incorporate these mechanisms in dislocation dynamics (DD) simulations which constitute the most suitable tool to study the evolution of a whole dislocation population, and thus to model the plastic flow at a mesoscopic scale.

Dislocation climb was introduced in several two- [6–8, 10] and three-dimensional (3D) [11–16] DD simulations. These models generally treat dislocation climb as a glide motion, *i.e.* a conservative motion, with a smaller mobility. This is not sufficient to capture all the involved physics. When the point defect concentration

---

\*Corresponding author. Email: emmanuel.clouet@cea.fr

in the bulk is different from its equilibrium value (e.g. under irradiation or after a quench of the crystal), dislocations can climb without the existence of a mechanical force. Point defect super- or under-saturation gives birth, in this case, to an additional force, the osmotic force. This is not described in simulations where climb is treated like glide, and only DD models based on the diffusion theory of point defects [14–18] lead then to a proper description of dislocation climb.

We introduce in the present article a diffusion based climb model in 3D DD simulations using a nodal representation of dislocations [19, 20]. The climb model is similar to the one previously used by Mordehai *et al.* [15, 16] in 3D DD simulations where dislocations were discretized in edge and screw segments. These DD simulations are used to study the coarsening kinetics of prismatic dislocation loops.

Prismatic dislocation loops, whose Burgers vector has a component normal to their habit plane, may be obtained in both thermal quenching [21, 22] and irradiation experiments [23–26]. They result from the condensation of point-defects, vacancies or interstitials, into discs which collapse to form a dislocation loop. These loops contribute in irradiated metals to the material embrittlement by radiation damage. In semiconductors, loops formed during the annealing stage which follows ion implantation may affect electronic properties of the device [27–29]. Knowing the long term time evolution of the loop population is therefore essential.

It has been observed experimentally [22, 24, 28–32] that loops coarsen: large loops grow at the expense of the smaller ones. Their size thus increases on average, whereas their density decreases. Different mechanisms for loop coarsening have been proposed and modeled. Large loops may grow by the absorption of vacancies emitted by the shrinking loops, the exchange being carried out through vacancy bulk diffusion [22, 24, 28, 32–36]. Pipe diffusion of point defects along the dislocation lines may also lead to a transfer of matter around the loops. This generates a translation of the loop in its habit plane, a process known as self climb or conservative climb [37]. Coarsening can then occur by direct coalescence of the loops [24, 29, 30]. Finally, if loops are unfaulted, they can glide along their prismatic cylinder, thus also allowing for coalescence [24]. Depending of the material, the type of the loops (vacancy or interstitial, faulted or unfaulted), and the annealing temperature, loop coarsening occurs by one or several of the mechanisms described above. In the present article, we do not consider pipe diffusion, which will be devoted to future work, and we study loop coarsening controlled by bulk diffusion. This coarsening regime has been reported in several experiments [28, 32, 34].

The paper is organized as follows. In the next section we describe our climb model and its introduction in 3D DD simulation. Then simulations of loop coarsening are performed, where prismatic glide of the loop is forbidden. This allows a comparison with the coarsening model first proposed by Kirchner [33], and revisited by Burton and Speight [35]. Finally, the contribution of prismatic glide to the kinetics is presented. The paper ends with concluding remarks.

## 2. Dislocation climb model

The climb model used in our DD simulations is based on the diffusion theory of point defects. As our DD simulations are used to study the annealing kinetics of post-irradiated or quenched materials, only vacancies are contributing to dislocation climb. Interstitials play a role only under irradiation. Jogs and pipe-diffusion are not considered in our model. This means that dislocations are assumed to be perfect sinks for vacancies which are thus at equilibrium all along the dislocation lines and not only on localized points corresponding to the jogs. These are the same assumptions as in the work of Mordehai *et al.* [15], where it has been shown that

such an idealized model leads nevertheless to a reasonable description of dislocation climb and is justified for high temperatures like the one of the present work (600 K in Al). In contrast with this earlier work, our DD simulations are based on a nodal representation of the dislocation line and not on a discretization in edge and screw segments. We therefore avoid discretization problems<sup>1</sup>, but we need to define a climb velocity for all the dislocation characters, and not only for the edge ones.

### 2.1. Climb mobility law

The starting point to derive the dislocation climb rate is the diffusion equation for the vacancy concentration  $c$  in the steady-state limit. Neglecting the elastic interaction between vacancies and dislocations, this reduces to the Laplace equation,

$$\Delta c(\mathbf{r}) = 0. \quad (1)$$

In order to obtain simple analytical expressions, we derive the solution of this equation for an isolated infinite straight dislocation. We therefore do not consider the interaction between the diffusion fields of the individual dislocation segments.

A cylindrical control volume with inner radius  $r_c$  of order of the core radius is defined around the dislocation segment whose climb rate we want to calculate. As we are not taking into account jogs nor pipe-diffusion, vacancies which diffuse into this control volume are absorbed immediately. At the distance  $r_c$  from the line, they are at equilibrium with the dislocation. This leads to a vacancy concentration [17, 38]

$$c_{\text{eq}} = c_0 \exp\left(\frac{F_{\text{cl}}\Omega}{kTb \sin(\theta)}\right), \quad (2)$$

where  $c_0 = \exp[-(U_{\text{v}}^{\text{f}} - P\Delta V_{\text{v}})/kT]$  is the equilibrium vacancy concentration in the defect-free crystal at the pressure  $P$ ,  $\Omega$  is the atomic volume,  $\theta$  describes the dislocation character<sup>1</sup>, *i.e.* the angle between its line direction unit vector  $\zeta$  and its Burgers vector  $\mathbf{b}$ ,  $U_{\text{v}}^{\text{f}}$  is the vacancy formation energy and  $\Delta V_{\text{v}}$  the associated relaxation volume<sup>2</sup>,  $k$  is the Boltzman's constant and  $T$  is the temperature. The mechanical climb force  $F_{\text{cl}}$  is the projection of the Peach-Koehler force in the direction perpendicular to the dislocation glide plane [40],

$$F_{\text{cl}} = [(\boldsymbol{\sigma}\mathbf{b}) \times \zeta] \cdot \mathbf{n}, \quad (3)$$

where  $\boldsymbol{\sigma}$  represents the stress tensor acting on the dislocation segment. It is thus the combination of the stress created by all other segments present in the simulation and of the externally applied load. The hydrostatic part of this tensor,  $P = -1/3 \text{Tr}(\boldsymbol{\sigma})$ , gives the pressure controlling the vacancy equilibrium concentration in Eq. (2). The normal  $\mathbf{n}$  to the dislocation glide plane appearing in Eq. (3)

<sup>1</sup>In their work, Mordehai *et al.* needed to correct the climb velocity of the edge segments to consider the actual orientation of the dislocation line (§ 2.3 in Ref. [15]).

<sup>1</sup> $\theta$  is defined from  $\sin(\theta) = \|\mathbf{b} \times \zeta\|/b$ , as a consequence,  $\sin(\theta)$  is always positive.

<sup>2</sup>The pressure dependence [39, 40] of the equilibrium vacancy concentration is not considered in the present simulations where a relaxation volume  $\Delta V_{\text{v}} = 0$  is assumed.

is defined for non screw dislocation by the convention

$$\mathbf{n} = \frac{\mathbf{b} \times \zeta}{\|\mathbf{b} \times \zeta\|} = \frac{\mathbf{b} \times \zeta}{b \sin(\theta)}. \quad (4)$$

With such a convention, a dislocation emits vacancies when it climbs in the direction of  $\mathbf{n}$ , and absorbs vacancies otherwise.

The solution of Eq. (1) at distance  $r$  from the dislocation segment is obtained by imposing  $c(r = r_\infty) = c_\infty$  in the bulk, far from the dislocation, leading to

$$c(r) = c_\infty + (c_\infty - c_{\text{eq}}) \frac{\ln(r/r_\infty)}{\ln(r_\infty/r_c)}. \quad (5)$$

An infinitesimal dislocation segment of length  $\delta l$  emits vacancies with a rate given by

$$\begin{aligned} \delta N_v &= -2\pi r_c \delta l \frac{D_v}{\Omega} \frac{\partial c}{\partial r} \Big|_{r=r_c} \\ &= -2\pi \delta l \frac{D_v}{\Omega} \frac{c_\infty - c_{\text{eq}}}{\ln(r_\infty/r_c)}, \end{aligned} \quad (6)$$

where the vacancy bulk diffusion coefficient is given by

$$D_v = D_v^0 \exp\left(-\frac{U_v^d}{kT}\right) \quad (7)$$

with  $U_v^d$  being the vacancy migration energy and  $D_v^0$  a constant pre-factor characterizing vacancy diffusion. If  $\delta N_v < 0$ , the segment actually absorbs vacancy. Its climb velocity  $\mathbf{v}_{\text{cl}} = v_{\text{cl}} \mathbf{n}$  is given by

$$\begin{aligned} v_{\text{cl}} &= \delta N_v \frac{\Omega}{b \delta l \sin(\theta)} \\ &= \frac{2\pi D_v c_0}{b \sin(\theta) \ln(r_\infty/r_c)} \left[ \frac{c_{\text{eq}}}{c_0} - \frac{c_\infty}{c_0} \right]. \end{aligned} \quad (8)$$

Eq. (8) actually gives the climb rate of the infinitesimal dislocation segment of length  $\delta l$ . We need to deduce from it the velocity of the nodes. This is done using “shape functions” [19, 20], *i.e.* functions which are non-zero only when a spatial point lies on the segment connected to a given node. This allows to define nodal forces by integration along each segment of the forces acting on this segment. This integration is done using 5 Gauss points on each segment with weights given by the shape function. The nodal velocities are obtained by solving the set of equations that link the nodal forces to the nodal velocities [19, 20], using mobility laws such as the one given by Eq. (8). This is more easily done if the velocity varies linearly with the applied force. We therefore linearized Eq. (8) by taking advantage that the climb force  $F_{\text{cl}}$  is small enough so that the exponential appearing in Eq. (2) can be expanded to the first order. This leads to the linear relation

$$v_{\text{cl}} = M_{\text{cl}}[F_{\text{cl}} + F_{\text{os}}], \quad (9)$$

where we have defined the climb mobility

$$M_{\text{cl}}(\theta) = \frac{2\pi D_v \Omega c_0}{kT b^2 \sin^2(\theta) \ln(r_\infty/r_c)}, \quad (10)$$

and the osmotic force [38–40]

$$\mathbf{F}_{\text{os}}(\theta) = \frac{kT}{\Omega} \left( 1 - \frac{c_\infty}{c_0} \right) b \sin(\theta) \mathbf{n}. \quad (11)$$

With this force, dislocations are climbing in presence of a vacancy supersaturation.

Considering that each point along the dislocation line may act as a sink or source of vacancies, and thus neglecting the effect of jogs and pipe-diffusion, implies that the climb mobility and the osmotic force depend only on the dislocation character,  $\theta$ . As seen from Eq. (11), the osmotic force tends to zero for a dislocation of screw character: a point defect supersaturation does not exert any force on a pure screw dislocation. But the climb mobility given by Eq. (10) is diverging for a screw dislocation. If the Peach-Koehler force has a component perpendicular to the dislocation glide plane<sup>1</sup>, our model leads to an infinite climb velocity for a screw dislocation. This artifact is usual in models where a climb mobility is defined for all dislocation characters [17] without incorporating jogs in the modeling. A proper account of the interaction between a vacancy and a jog in the case of a screw orientation, may remove the divergence of the climb mobility. In the present work, the divergence is handled by considering that screw dislocations do not climb. We therefore enforce zero climb velocity for all segments which are nearly parallel with their Burgers vector. When the dislocation character  $\theta$  is less than  $10^{-6}$  radians, the segment is handled in our code as pure screw. We check that varying this threshold does not change the results of our simulations.

The incorporation in the diffusion equation (1) of the elastic interaction between vacancies and dislocations will change the climb mobility (10) by multiplying it with a prefactor depending on the interaction energy and the temperature [41]. It will therefore only lead to a correction on the time scale. Such an elastic interaction is important to consider when two different point defects, like vacancies and interstitials, are diffusing as it can lead to some bias on their relative absorption by dislocations [41]. In our simulations, only vacancies are present and we therefore neglect the effect of this elastic interaction.

## 2.2. Simulation setup

For simulations the materials parameters of fcc aluminum are used: lattice constant  $a = 0.404$  nm, shear modulus  $\mu = 26.5$  GPa, Poisson coefficient  $\nu = 0.345$ , vacancy migration energy  $U_v^d = 0.61$  eV, vacancy formation energy  $U_v^f = 0.67$  eV, atomic volume  $\Omega = 16.3 \times 10^{-30}$  m<sup>3</sup>, diffusion coefficient pre-exponential  $D_0 = 1.18 \times 10^{-5}$  m<sup>2</sup>s<sup>-1</sup>.

At each simulation step, the stresses, forces, and velocities are calculated. No external loading is applied. Then the dislocations are moved using an integration time interval inversely proportional to the maximum velocity of all nodes. The nodes are allowed to fly over a maximum distance of one Burgers vector in case of

---

<sup>1</sup>As we are modeling climb in fcc crystals where dislocations are dissociated, the glide plane can be defined even for a screw dislocation although  $\mathbf{b} \times \boldsymbol{\zeta} = \mathbf{0}$  in this case.

glide motion and  $b/10$  in case of climb, this defining the duration of the time step for integration.

No image stress corresponding to free surfaces or periodic boundary conditions are considered. The stress field calculation therefore assumes that dislocations are in an infinite homogeneous elastic medium. The stress calculation is performed using the non singular expressions of Cai *et al.* [42] assuming isotropic elasticity with a parameter  $a = 3 \text{ \AA}$  for the core spreading.

For the numerical simulations of prismatic loop coarsening, the loops are of vacancy type and we assume that they are far enough from surfaces and grain boundaries, so that the loops are the only sources and sinks for vacancies. The total number of vacancies in the system, *i.e.* the sum of vacancies condensed in the loops and the free vacancies diffusing in the bulk, is therefore a conserved quantity. Climbing dislocations emit or absorb a number of vacancies proportional to the area they sweep. The vacancies in the bulk are considered to reach steady state instantaneously. The time evolution of the bulk vacancy concentration is then governed by the equation

$$\frac{dc_{\infty}}{dt} = \frac{b}{V} \frac{dS}{dt}, \quad (12)$$

where  $V$  is the volume of the sample and  $S$  is the area swept by the loops during climb. If a dislocation segment  $\delta l$  climbs a distance  $v_{cl} \Delta t$ , the corresponding swept area is given by  $\delta S = v_{cl} \Delta t \delta l \sin(\theta)$ . The sign of the climbing velocity fixes the sign of the swept area and therefore determines if the dislocation segment is absorbing ( $\delta S < 0$ ) or emitting vacancies ( $\delta S > 0$ ).

### 3. Climb-only controlled coarsening

#### 3.1. DD simulations of loop coarsening

We first use the climb model to simulate the coarsening kinetics of prismatic loops which are not allowed to glide, thus putting the glide mobility to zero in the DD simulations. This corresponds to the behavior of faulted loops which cannot glide on their prismatic cylinder because of the existing stacking fault. The additional force exerted by the stacking fault on the dislocation segments is not included in the simulation.

The initial configuration is a population of circular loops which are placed at random in a box of size  $L \times L \times L$ ,  $L = 2 \mu\text{m}$ , and with the condition that they do not overlap and the disks corresponding to them do not intersect. Their habit planes are also chosen at random from the plane family  $\{110\}$ . The Burgers vector of the loops is of  $1/2 \langle 110 \rangle$  type and is perpendicular to the loop habit plane. The loops are then pure prismatic. As glide is not allowed, they can only grow or shrink in their habit plane by climb. As a consequence, they remain pure prismatic during the whole simulations. This means that all the dislocation segments are pure edge. These loops are of vacancy type and thus the glide plane normal  $\mathbf{n}$ , as defined by Eq. (4), is pointing at every point to the center of the loop.

We set the temperature to a constant value,  $T = 600 \text{ K}$ , during the simulation, and we start with no vacancy supersaturation:  $c_{\infty}(t = 0) = c_0$ . For a short time at the beginning, all loops start shrinking because of their line tension and emit vacancies. As a result, the vacancy concentration  $c_{\infty}$  in the bulk increases. This transient regime occurs because  $c_0$  is the equilibrium vacancy concentration in a defect-free crystal. Because of the line tension of the loops and of the associated

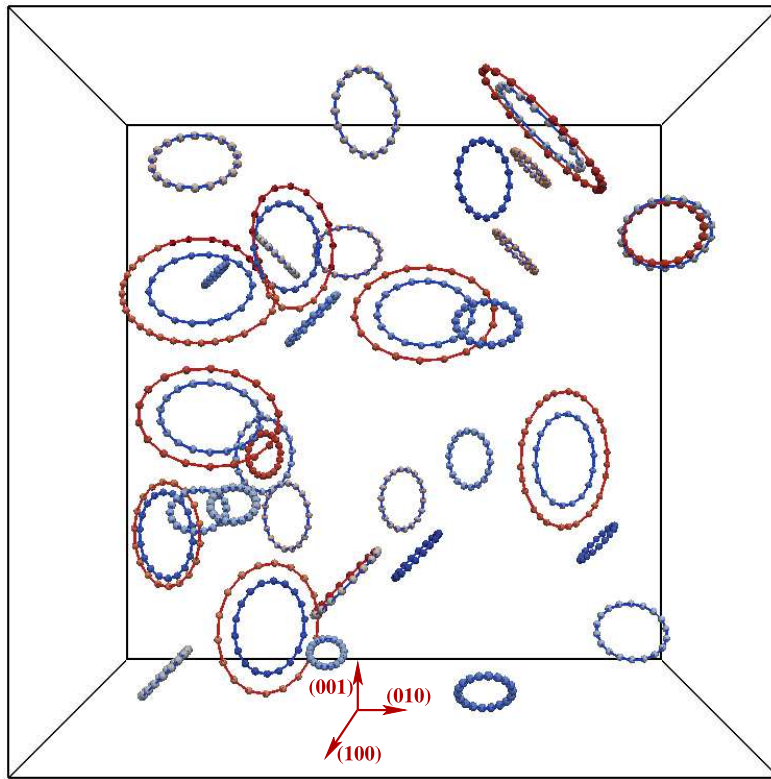


Figure 1. [Color online] Typical configuration of loops, when glide is not possible. Darker [blue] lines represent the loops at  $t = 0$  and lighter [red] lines at  $t = 1$  s. (See video as supplementary online material.)

Gibbs-Thomson effect, the vacancy concentration in equilibrium with the vacancy prismatic loops needs to be higher than  $c_0$ . This vacancy supersaturation creates an osmotic force. The coarsening kinetics will then result from the competition between this osmotic force and the mechanical climb force. For small loops, the line tension leads to a mechanical climb force higher than the osmotic force, thus making the loops shrink. Larger loops have a smaller line tension. Therefore the osmotic force is higher than the mechanical climb force for them. The larger loops grow then by absorbing the vacancies emitted by the smaller ones which are shrinking. The frontier between stable and unstable loops is controlled by the instantaneous vacancy concentration  $c_\infty(t)$  through the Gibbs-Thomson effect. As  $c_\infty(t)$  is tending to  $c_0$  with the time evolution, this frontier is going to the larger sizes of the loops. As a consequence, as time evolves, the loops grow on average in radius whereas their density decreases. A typical configuration at  $t = 0$  and time  $t = 1$  s is shown in Figure 1.

### 3.2. Coarsening kinetics

To extract quantitative information from our DD simulations, we consider 500 statistically equivalent systems with different realization of randomness. The prismatic loops at  $t = 0$  have random radii generated with uniform distribution, with the constraint that their total area at  $t = 0$  is the same in all simulations. Simulations have been performed for three different initial total loop areas  $S(0) = L^2/4$ ,  $S(0) = L^2/2$ ,  $S(0) = L^2$ , where  $L$  is the size of the simulation box. The time evolution of the average radius  $R_{av}$  of the loops, of the average number of loops  $N_{loops}(t)$  in the simulation box, and of the vacancy supersaturation  $c_\infty(t)/c_0$  in the bulk is respectively shown in Figure 2, 3, and 4.

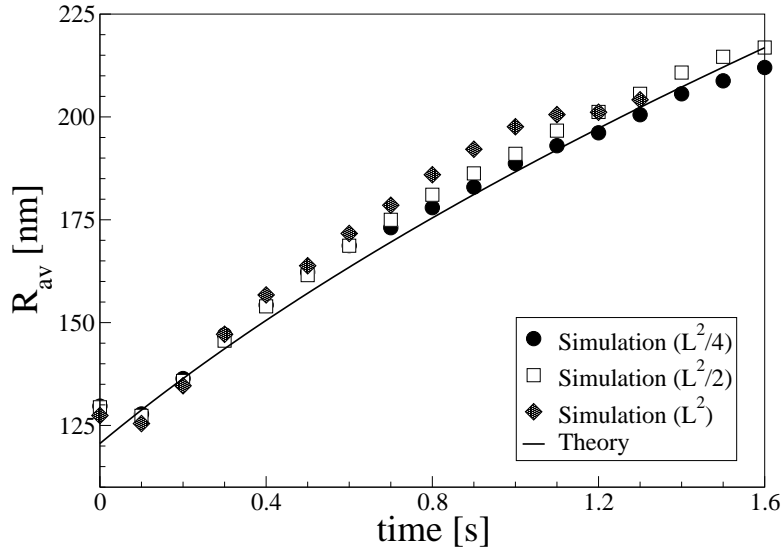


Figure 2. Time evolution of the average radius of the loops for three different initial total areas  $L^2/4$ ,  $L^2/2$ , and  $L^2$ . The line corresponds to Eq. (13).

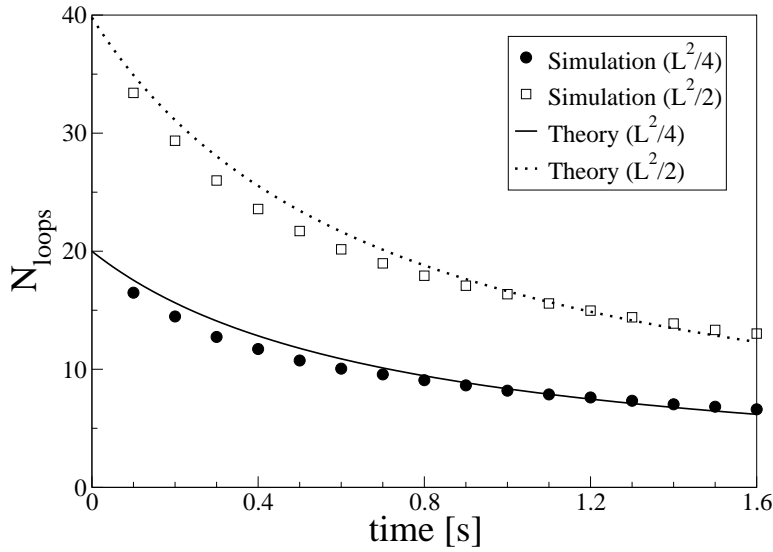


Figure 3. Time evolution of the average number of loops for two different total initial areas  $L^2/4$  and  $L^2/2$ . The lines correspond to Eq. (15).

Kirchner [33] and Burton and Speight [35] have modeled the coarsening kinetics for prismatic dislocation loops (KBS model). Their model is based on the line tension approximation for the loops and uses the same assumptions as in our DD simulations: loops cannot glide and only vacancy bulk diffusion makes the loops grow or shrink. A good agreement has been observed with experimental data [28, 32, 34] when these assumptions are valid. We check, in the present work, if such an agreement can also be obtained with our DD simulations.

According to this coarsening model, the average radius of the loops  $R_{av}(t)$  should increase like  $t^{1/2}$ , following the law

$$R_{av}(t) = R_{av}(0)[1 + \alpha t]^{1/2}, \quad (13)$$



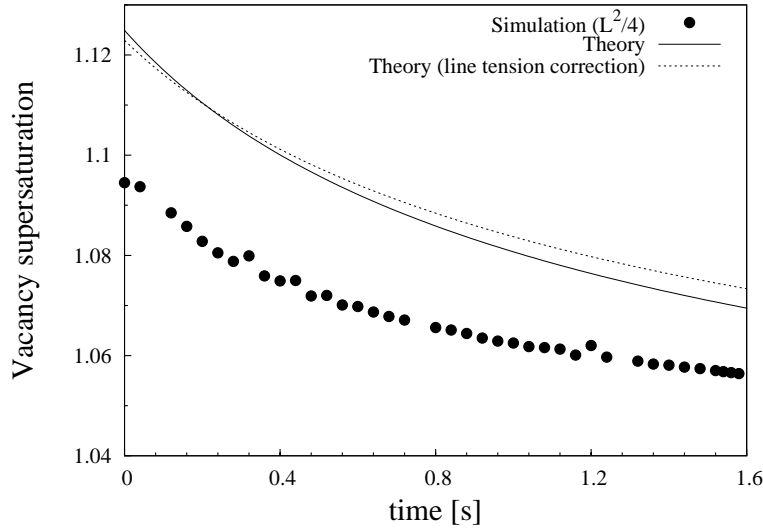


Figure 4. Time evolution of the vacancy supersaturation,  $c_\infty(t)/c_0$ , for the initial total loops area  $L^2/4$ . The lines are predictions of the KBS model for different line tension approximations. The solid line corresponds to Eq. (16) where the line tension is  $\mu b/R$ . The dashed line corresponds to Eq. (18) where the line tension is given by Eq. (17) with  $r_c = 1.5 \text{ \AA}$ .

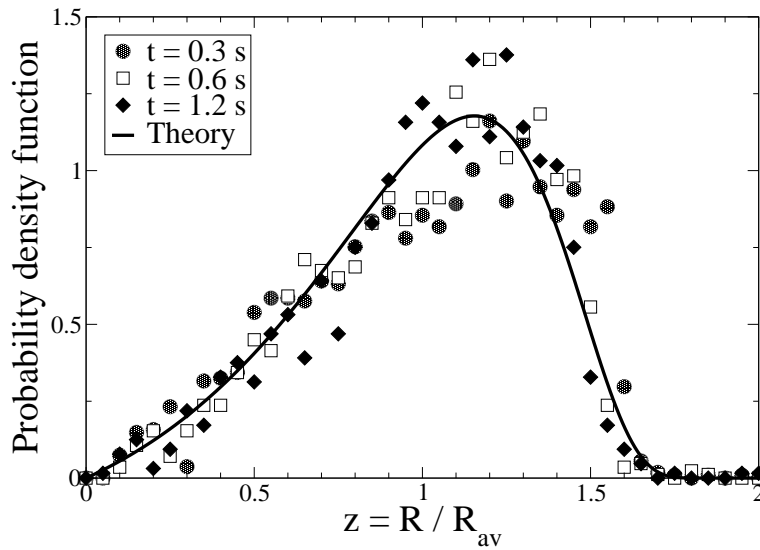


Figure 5. Probability distribution function of the normalized loop sizes for the initial total loops area  $L^2/4$ .

where the temperature dependent growth rate is given by

$$\alpha = \frac{\eta}{2R_{av}^2(0)} \frac{c_0 D_v \mu \Omega}{kT}. \quad (14)$$

Here  $\eta$  is a geometric factor depending on the approximation used and on the boundary conditions when solving the vacancy diffusion equation for an isolated loop. Burton and Speight [35] assumed that the loops are acting as a point source / sink for vacancies and obtained  $\eta = 2$ . This value has been found in good agreement with the one derived from our DD simulations of the shrinkage of an isolated loop (*cf* Appendix A). We therefore use this value. Using in Eq. 14 the input parameters of our DD simulations, we compare the time evolution of the loop average radius

observed in our DD simulations with the one predicted by Eq. (13). Figure 2 shows that a quantitative agreement is obtained for all the initial loop areas studied. As predicted by the KBS model, the average size of the loops only depends on its initial value and not on the loop density.

The KBS model predicts that the number of loops  $N_{\text{loops}}(t)$  decreases like the inverse of the time:

$$N_{\text{loops}}(t) = \frac{N_{\text{loops}}(0)}{1 + \alpha t}. \quad (15)$$

This is in perfect agreement with the results obtained in our DD simulations (Figure 3).

The vacancy supersaturation is directly linked to the average size of the loops according to the KBS model:

$$\frac{c_{\infty}(t)}{c_0} = 1 + \frac{\mu b \Omega}{kT R_{\text{av}}(t)}. \quad (16)$$

It should therefore decay asymptotically like  $t^{-1/2}$ . The agreement with our DD simulations is not as perfect as for  $R_{\text{av}}(t)$  and  $N_{\text{loops}}(t)$ , but the discrepancy is nevertheless small (Figure 4). This difference may arise from the line tension approximation used in the KBS coarsening theory where it is assumed that a loop of radius  $R$  is subject to the stress  $\tau = \mu b/R$ . A more precise expression of the line tension exist for a circular prismatic loop [43]. Such a loop of radius  $R$  is indeed subject to the self stress

$$\tau(R) = \frac{\mu b}{4\pi(1-\nu)R} \log\left(\frac{4R}{r_c}\right). \quad (17)$$

The core radius  $r_c$  appearing in this expression is directly linked to the parameter  $a$  used to spread dislocation core in the non singular expressions of the stress field [42]. For a prismatic loop, one should take  $r_c = a/2$ , *i.e.* 1.5 Å in our case. With this value of the core radius,  $\tau(R)R/\mu b$  varies between 0.96 and 1.08 for loop radii between 100 and 250 nm. This shows the correctness of the approximation used by Kirchner [33] and Burton and Speight [35] for the line tension. This small difference on the value of the line tension only slightly impact the vacancy supersaturation. Using Eq. (17) for the line tension instead of  $\mu b/R$ , the time evolution of the vacancy supersaturation is given by

$$\frac{c_{\infty}(t)}{c_0} = 1 + \frac{\mu b \Omega}{4\pi(1-\nu)kT R_{\text{av}}(t)} \log\left(\frac{4R_{\text{av}}(t)}{r_c}\right). \quad (18)$$

Figure 4 shows that the change on the vacancy supersaturations is small in the considered size range. This does not really improve the agreement with our DD simulations. Probably, even Eq. (17) based on an improved line tension approximation only roughly estimates the stress existing on the dislocation segments in the DD simulations. Eq. (17) assumes that the loops are circular and neglect the interaction between different loops: DD simulations do not make these approximations. On the other hand, one cannot exclude that the discretization of the loops in our DD simulations induces a noise on the line tension which may impact the vacancy supersaturation. For instance, 5 Gauss points on each segment were used to integrate forces on each segment so as to obtain nodal forces. A better estimation of the line tension may require more Gauss points or an analytical expression of

the nodal forces [20]. Despite all these limitations on the comparison between the results of our DD simulations and the predictions of the KBS model, the agreement on the vacancy supersaturation is reasonable.

Finally, the KBS theory predicts that the size distribution of the loops, once normalized, is stationary and is given by

$$g(z) = \frac{1}{8e^2} \frac{z}{(z-2)^4} \exp\left(\frac{4}{z-2}\right) \quad (19)$$

if  $0 < z < 2$ , and 0 otherwise.  $z = R/R_{av}(t)$  is a normalized radius and  $g(z)dz$  is the probability to find a loop with a normalized size between  $z$  and  $z + dz$ . The normalized size distribution in our DD simulations is stationary and perfectly obeys Eq. (19), as can be seen in Figure 5.

A perfect agreement is therefore obtained between the simulations and the coarsening model for prismatic loops of Kirchner [33] and Burton and Speight [35]. The agreement shows that this model is well suited when studying the coarsening of loops by vacancy bulk diffusion.

#### 4. Contribution of glide to the loop coarsening

The advantage of DD simulations is that they are not restricted to the study of climb associated with bulk diffusion. We can superpose dislocation glide to see how it affects loop coarsening. Loops are able to glide if they are unfaulted. One observes then experimentally [24] a faster coarsening kinetics than with only bulk diffusion.

##### 4.1. Combining climb and glide motion

The drag coefficient, the inverse of the mobility, for dislocation glide is mainly controlled by phonon drag in pure fcc metals and varies linearly with the temperature. The temperature dependence in aluminum was obtained by molecular dynamics calculations by Kuksin and coworkers [44] who found

$$B_{gl}(T) = B_{gl}(300\text{ K}) \frac{T}{300}, \quad (20)$$

where  $B_{gl}(300\text{ K}) = 1.4 \times 10^{-5} \text{ Pa}\cdot\text{s}$  is the value of the drag coefficient at temperature 300 K. This value lies in between the two available experimental data  $B_{gl}(300\text{ K}) \approx 0.6 \times 10^{-5} \text{ Pa}\cdot\text{s}$  (Ref. [45]) and  $B_{gl}(300\text{ K}) \approx 2.6 \times 10^{-5} \text{ Pa}\cdot\text{s}$  (Ref. [46]), and is also close to other molecular dynamics simulation results by Olmsted and coworkers [47],  $B_{gl}^{\text{edge}} = 1.2 \times 10^{-5} \text{ Pa}\cdot\text{s}$  and  $B_{gl}^{\text{screw}} = 2.2 \times 10^{-5} \text{ Pa}\cdot\text{s}$  at 300 K, and Groh and coworkers [48],  $B_{gl}(300\text{ K}) = 4.5 \times 10^{-5} \text{ Pa}\cdot\text{s}$ . For simplicity, we neglect in our simulations that screw segments glide slower than edge segments and we consider a drag coefficient for glide which does not depend on the dislocation character, as given by Eq. (20).

The important point is that the glide mobility is much higher than the climb mobility at the considered temperatures. At 600 K, the glide mobility is  $M_{gl} = 3.3 \times 10^5 \text{ Pa}^{-1}\cdot\text{s}^{-1}$ , whereas the climb mobility for edge dislocations is only  $M_{cl} = 1.75 \times 10^{-5} \text{ Pa}^{-1}\cdot\text{s}^{-1}$ . Due to this difference of 10 orders of magnitudes between both mobilities, it is not possible to handle both dislocation motions in the same step in our DD simulations. The time interval compatible with the glide mobility

would be so small that no climb could be observed during this period.

We therefore perform the glide and climb motions separately with two different time steps, using an adiabatic approximation which assumes that the degrees of freedom corresponding to dislocation glide reach an equilibrium between two successive climb events. The dislocation microstructure is equilibrated first with respect to the glide motion. Once glide is not producing any plastic strain, one climb step is performed: the glide mobility is put to zero and the time step is set to a value compatible with the climb mobility. After this climb event, we equilibrate again the dislocation microstructure with respect to glide and then go back to climb, thus cycling between climb events and glide equilibration. The dislocations are considered to be in equilibrium with the glide motion, when the relative difference in the change of the Frobenius norm of the plastic strain tensor  $\varepsilon$  between two consecutive time steps is less, than  $10^{-3}$ . Assuming index notation this can be expressed as

$$\left| 1 - \frac{\sqrt{\varepsilon_{ij}(t+dt)\varepsilon_{ij}(t+dt)}}{\sqrt{\varepsilon_{ij}(t)\varepsilon_{ij}(t)}} \right| < 10^{-3}. \quad (21)$$

We check that the result of our simulations does not depend on the value of this threshold by performing some simulations also with a  $10^{-4}$  threshold.

Finally, one should stress that the definite  $\{111\}$  initial glide planes are lost in our DD simulations. A climbing dislocation is jogged. It therefore, does not lie, on average, in a definite  $\{111\}$  plane. The nodal representation of the dislocation lines does not describes all jogs existing on the dislocation, but ‘‘coarse-grains’’ the line to use less nodes per dislocation length. As a consequence, the dislocation line vector  $\zeta$  may lie in a plane different from a  $\{111\}$  plane. The dislocation glide plane is then fixed by this line vector  $\zeta$  and the Burgers vector  $\mathbf{b}$ . The mobility of the jogged dislocation should be smaller than the one of the perfect dislocation as revealed by atomic simulations [49]. Nevertheless, this is negligible compared to the mobility difference between glide and climb. We therefore do not consider the effect of jogs on the glide mobility. This is different from the picture of a jogged dislocation in DD simulations where dislocations are discretized in edge and screw segments [15, 16]: in such simulations, all segments belong to a definite  $\{111\}\langle 110 \rangle$  glide system, but the jogs have to be concentrated in a single point instead of being spread all along the dislocation line, thus creating a superjog in the simulation.

#### 4.2. *Glide and loop coarsening*

When the glide mobility is non-zero, prismatic loops can glide on the surface of a cylinder, whose axis is parallel to the Burgers vector of the loops. Due to the elastic interactions between them, loops move on this prismatic cylinders. The first consequence is that they can deviate now from their pure edge orientation. Most importantly, if the cylinders of two different loops intersect, the loops can come into contact with each other. Loops can thus merge by gliding on their prismatic cylinder, a process much faster than coarsening by bulk diffusion. This is illustrated in Figure 6 which shows the time evolution of a system formed by two attracting prismatic loops. The two circular loops at  $t = 0$  (Figure 6a) approach each other in a short time by gliding on their prismatic cylinders (Figure 6b) until they come in contact and reach an equilibrium configuration (Figure 6c). They then climb, the largest loop absorbing the vacancies emitted by the smallest one (Figures 6d-6f). During all this coalescence stage, glide allows the loops to keep their equilibrium shape. At the end (Figure 6f), only the largest loop survives. The coarsening thus

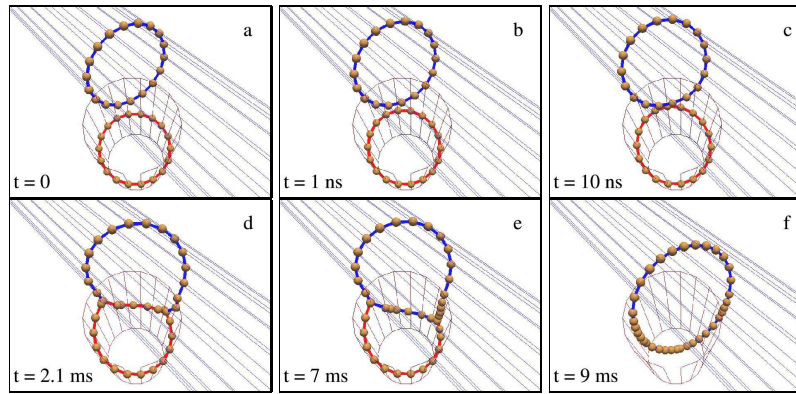


Figure 6. [Color online] Coarsening of a system formed by two attracting loops gliding on prismatic cylinders which intersect each other. The initial glide cylinders of both loops are sketched with thin lines. The axis of these cylinders correspond to the Burgers vector of the loops which are  $a/2[101]$  and  $a/2[\bar{1}10]$  respectively for the red and the blue loops. The Burgers vector of the junction that can be seen in the insets d and e is  $a/2[011]$ . The initial radius of the red loop is  $r = 210$  nm and of the blue loop  $r = 230$  nm.

results from climb assisted by glide. One should also note that, in this case, the loops are so close that the mechanical climb force does not only arises from the loop line tension but also from the stress exerted from one loop to the other. This is another factor, associated with loop glide, which leads to a speed-up of the coarsening.

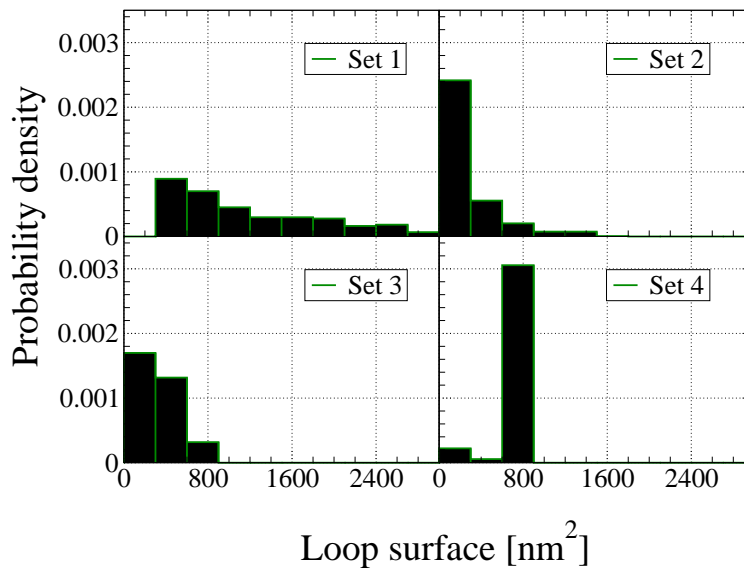


Figure 7. Initial probability density distribution of loop surfaces for the simulations with glide and climb.

The influence of the glide on the time evolution of the quantities of interest (vacancy supersaturation, loop density, mean projected loop area) was studied on four different sets of loops. The initial size distributions corresponding to the four different sets of simulations are presented in Figure 7. All sets contain the same number of vacancies condensed in the loops, but some sets correspond to a high density of small loops (sets 2 and 3), whereas some other sets to a broader distribution with larger loops and a smaller density (set 1). The side of the simulation box was set to  $L = 500$  nm and the statistics was obtained by averaging over 50 statistically equivalent simulations. Initially no vacancy supersaturation exists in the simulation box ( $c_\infty(t = 0) = c_0$ ). The area of the loops was calculated by

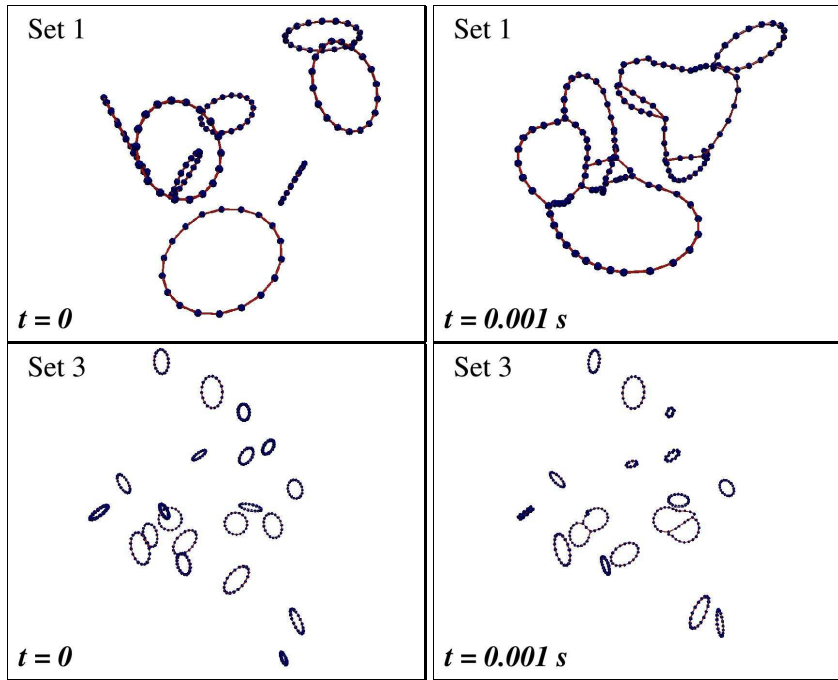


Figure 8. [Color online] Coarsening dynamics of loops in a typical simulation for Set 1 (top) and Set 3 (bottom). (See video as supplementary online material.)

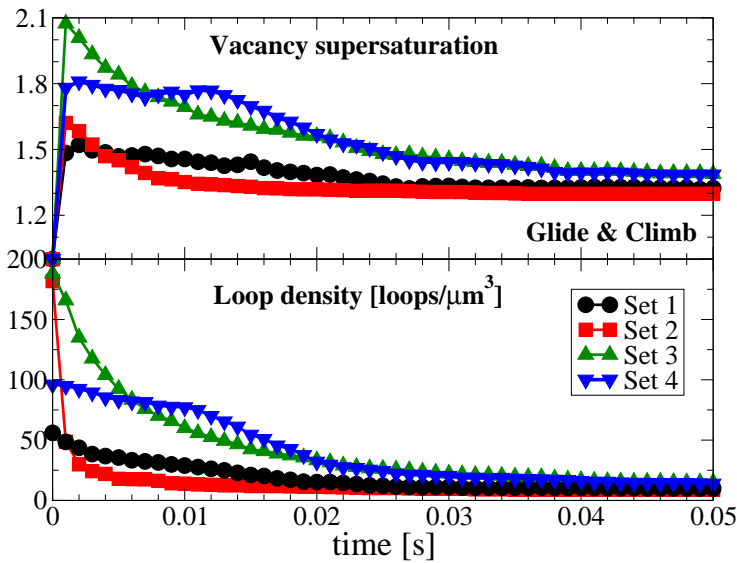


Figure 9. [Color online] Time evolution of the vacancy supersaturation  $c_{\infty}(t)/c_0$  and of the loop density in the simulations with glide and climb.

projecting the loops on planes perpendicular to the Burgers vector of the loops. It gives thus a measure of the number of vacancies condensed in the loops.

Glide makes the loop population rapidly evolve at the beginning of the simulation. In set 1, which contains large loops close to each other, loops come in contact by glide and form a complicated network (Figure 8) which then evolves by climb assisted by glide. In contrast, in set 3, which is a collection of small loops separated by larger distances compared to their radius, few loops coalesce by glide at the beginning. The coarsening mainly proceed by climb, with glide leading to some isolated coalescence events and thus enhancing the kinetics.

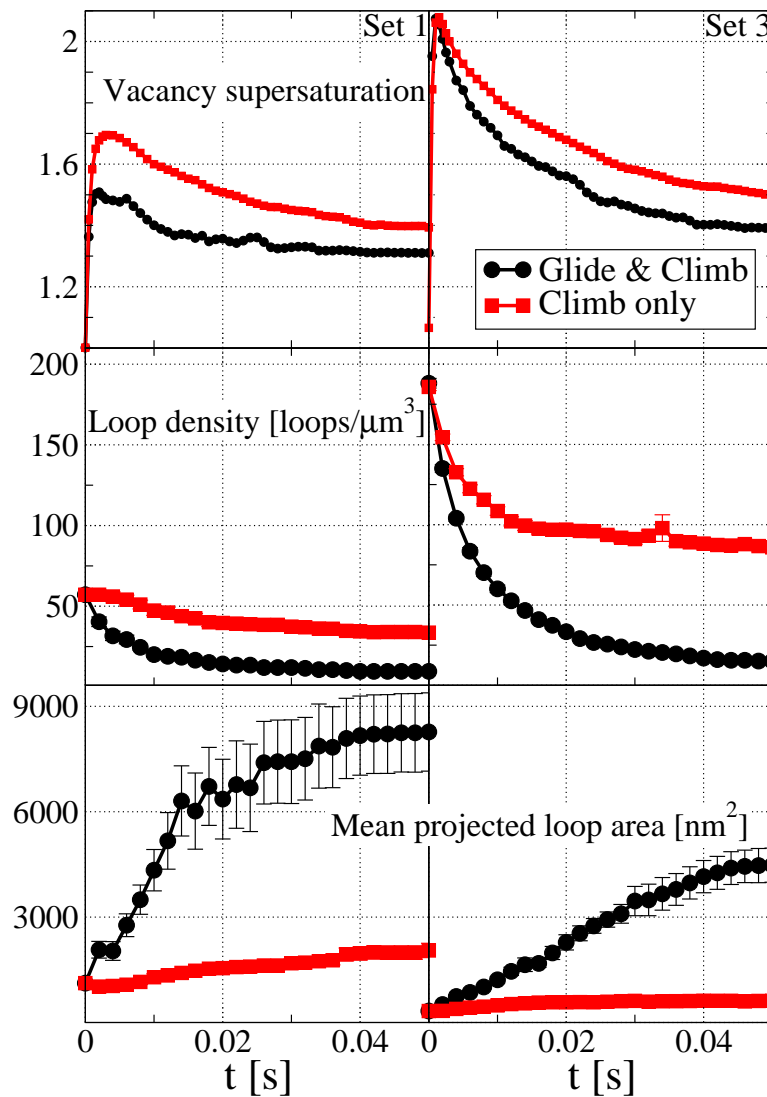


Figure 10. [Color online] Time evolution of the vacancy supersaturation, loop density, and mean projected loop area in the simulations with finite glide drag coefficient, compared to the simulations with infinite glide drag coefficient, for the data set 1 (on the left) and data set 3 (right column).

The time evolution of the vacancy supersaturation and of the loop densities is presented in Figure 9. The vacancy supersaturation initially increases for short time so as to reach equilibrium with the given loop population. This is similar to what was observed in the previous section without glide. Then the supersaturation decays as the loops absorb the excess of vacancies during the coarsening, whereas the loop density decreases and their size increases.

To highlight the effect of glide on the coarsening of the prismatic loops, the simulations were repeated on the data sets 1 and 3, with a glide mobility set to zero. As it can be seen from Figure 10, the simulations with glide and climb result in faster coarsening than simulations with climb only. Of course, when loops are allowed to glide, the coarsening model of Kirchner [33] and Burton and Speight [35] does not apply anymore. This is quite normal as this model assumes that loops can only climb thanks to vacancy bulk diffusion and, as soon as loop glide is allowed, it dramatically changes the coarsening kinetics.

## 5. Conclusion

The introduction in DD simulations of a dislocation climb model based on vacancy bulk diffusion allows us to study the coarsening kinetics of prismatic loops. When loops cannot glide, because they are faulted for instance, we obtain a perfect agreement between our simulations and the coarsening model of Kirchner [33] and Burton and Speight [35]. The average size of the loops increases with time  $t$  like  $t^{1/2}$ , the loop density decreases like  $1/t$ , and the vacancy supersaturation decreases like  $t^{-1/2}$ .

When the loops can also glide on their prismatic cylinders, a much faster coarsening kinetics is obtained. Prismatic glide leads to direct coalescence of the loops. These coalescence events enhance the coarsening of the loop distribution. For high loop densities, where the distance between loops is small compared to their size, glide leads to a complex dislocation microstructure and coarsening mainly proceeds by aggregation.

Only vacancy bulk diffusion has been taken into account in our simulations. It has been proposed in the literature [30] that vacancy pipe-diffusion also leads to coalescence of the loops, as a result of a motion of the loops in the plane perpendicular to their prismatic cylinder. The next step of this work will therefore be to include climb associated with vacancy pipe diffusion so as to simulate all coarsening regimes. The effects of jogs on climb [50] should also be considered so as to improve the climb mobility law.

## Acknowledgments

This work was supported by the European fusion materials modeling program (EFDA MAT-REMEV). The simulations were performed with the 3D DD code Numodis (CEA-CNRS, France). The authors are grateful to the other developers of the code, M. Fivel, E. Ferrie, and V. Quatella.

## Appendix A. Isolated loop

The coarsening model of Kirchner [33] and of Burton and Speight [35] makes use of the growing law of a prismatic loop. Such a law is based on the line tension approximation and on the solution of Fick's equation for vacancies diffusing from the bulk to the loop. Several solutions can be found in the literature depending of the assumed geometry for the flux fields and of the boundary conditions for the vacancy concentration. These solutions differ only in the value of the geometrical factor  $\eta$  which appears in Eq. (14) in the modeling of coarsening kinetics of prismatic loops. Seidman and Balluffi [51] assuming toroidal boundary conditions for the flux field around the prismatic loop obtained  $\eta(R) = \sqrt{6}\pi/\ln(8R/r_c)$ , where  $r_c$  is the circular cross-section of the torus and  $R$  is its radius. If the loop is treated as a disc [33], the value is  $\eta = 4/\pi\sqrt{3/2} \approx 1.56$ . Burton and Speight obtained  $\eta = 2$  by assuming spherical symmetry for the vacancy flux field around a loop considered to be a punctual source/sink.

Following the approach of Mordehai *et al.* [15], we use our DD simulations in combination with a line tension model to evaluate the value of  $\eta$ . We therefore simulate the loop shrinkage of an isolated loop under equilibrium vacancy concentration  $c_\infty = c_0$ , and we maintain fixed this vacancy concentration in the bulk. One observes that a vacancy loop annihilates. According to the line tension model



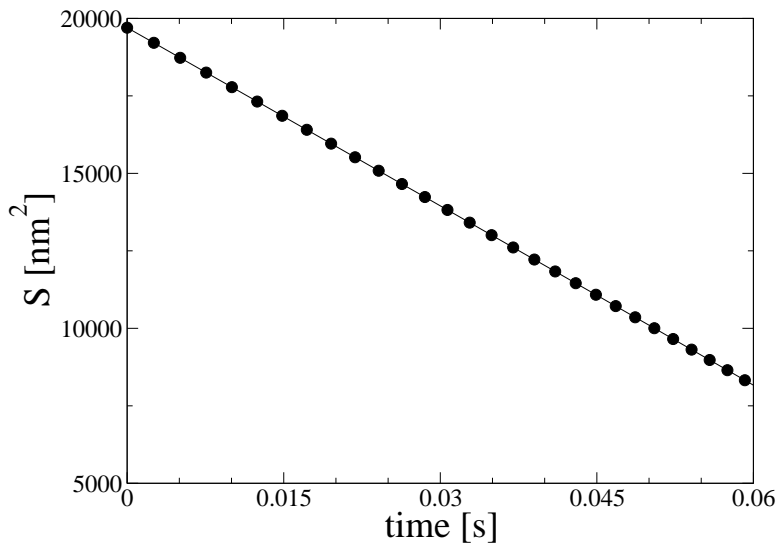


Figure A1. Time evolution of the surface  $S$  of an isolated loop with initial radius  $R(0) = 80$  nm when  $c_\infty(t) = c_0$ .

[15, 33, 35, 51] its surface  $S$  is decreasing like

$$S(t) = S_0 \left( 1 - \frac{t}{\tau_0} \right), \quad (\text{A1})$$

where  $S_0$  is the initial surface of the loop and the annihilation time  $\tau_0$  is given by

$$\tau_0 = \frac{kTS_0}{2\pi\eta c_0 D_v \mu \Omega}. \quad (\text{A2})$$

The shrinkage of an isolated loop with initial radius  $R(0) = 80$  nm is presented in Figure A1: the linear variation with time of the surface of the loop is clearly obtained. Using Eq. (A2), the value of the geometric factor  $\eta$  can be deduced. For loops with radius from  $R = 80$  nm up to  $R = 4 \mu\text{m}$ , we get values  $\eta \approx 1.92 - 1.98$ , close to the value  $\eta = 2$  obtained by Burton and Speight [35]. For the sake of simplicity we then also assume that  $\eta(R)$  is constant, and we use the value  $\eta = 2$ .

## References

- [1] D. Caillard and J.L. Martin, *Rev. Phys. Appl. (Paris)* 22 (1987) p.169–183.
- [2] J.P. Poirier *Creep of Crystals: High-Temperature Deformation Processes in Metals, Ceramics and Minerals*, Cambridge University Press, 1985.
- [3] F. Humphreys and M. Hatherly *Recrystallization and Related Annealing Phenomena*, Pergamon Press, Oxford, 1995.
- [4] P. Rudolph, *Cryst. Res. Technol.* 40 (2005) p.7.
- [5] P. Rudolph, C. Frank-Rotsch, U. Juda and F.M. Kiessling, *Mater. Sci. Eng. A* 400–401 (2005) p.170.
- [6] B. Bakó, I. Groma, G. Györgyi and G.T. Zimányi, *Comput. Mater. Sci.* 38 (2006) p.22.
- [7] B. Bakó, I. Groma, G. Györgyi and G.T. Zimányi, *Phys. Rev. Lett.* 98 (2007) p.075701.
- [8] B. Bakó and W. Hoffelner, *Phys. Rev. B* 76 (2007) p.214108.
- [9] B. Bakó and I. Groma, *Phys. Rev. Lett.* 84 (2000) p.1487.
- [10] F. Roters, D. Raabe and G. Gottstein, *Comp. Mater. Sci.* 7 (1996) p.56 – 62.
- [11] W. Cai and V.V. Bulatov, *Mater. Sci. Eng. A* 387–389 (2004) p.277 – 281.
- [12] Y. Xiang and D.J. Srolovitz, *Philos. Mag.* 86 (2006) p.3937–3957.
- [13] Z. Chen, K.T. Chu, D.J. Srolovitz, J.M. Rickman and M.P. Haataja, *Phys. Rev. B* 81 (2010) p.054104.
- [14] N.M. Ghoniem, S.H. Tong and L.Z. Sun, *Phys. Rev. B* 61 (2000) p.913–927.
- [15] D. Mordehai, E. Clouet, M. Fivel and M. Verdier, *Philos. Mag.* 88 (2008) p.899 – 925.
- [16] D. Mordehai, E. Clouet, M. Fivel and M. Verdier, *IOP Conf. Series: Mater. Sci. Eng.* 3 (2009) p.012001.
- [17] M.J. Turunen, *Acta Metall.* 24 (1976) p.463 – 467.
- [18] D. Raabe, *Philos. Mag. A* 77 (1998) p.751–759.

- [19] V.V. Bulatov and W. Cai *Computer simulation of dislocations*, Oxford University Press, New York, 2006.
- [20] A. Arsenlis, W. Cai, M. Tang, M. Rhee, T. Ooppelstrup, G. Hommes, T.G. Pierce and V.V. Bulatov, *Modelling Simul. Mater. Sci. Eng.* 15 (2007) p.553–595.
- [21] P.B. Hirsch, J. Silcox, R.E. Smallman and K.H. Westmacott, *Philos. Mag.* 3 (1958) p.897–908.
- [22] J. Silcox and M.J. Whelan, *Philos. Mag.* 5 (1960) p.1.
- [23] B.C. Masters, *Philos. Mag.* 11 (1965) p.881.
- [24] B.L. Eyre and D.M. Maher, *Philos. Mag.* 24 (1971) p.767.
- [25] B.L. Eyre, *J. Phys. F: Met. Phys.* 3 (1973) p.422–470.
- [26] H. Kawanishi, S. Ishino and E. Kuramoto, *J. Nucl. Mater.* 141-143 (1986) p.899 – 902.
- [27] K.S. Jones, S. Prussin and E.R. Weber, *Appl. Phys. A: Mater. Sci. Process.* 45 (1988) p.1 – 34.
- [28] C. Bonafos, D. Mathiot and A. Claverie, *J. Appl. Phys.* 83 (1998) p.3008–3017.
- [29] P.O.A. Persson, L. Hultman, M.S. Janson and A. Hallen, *J. Appl. Phys.* 100 (2006) p.053521.
- [30] C.A. Johnson, *Philos. Mag.* 5 (1960) p.1255–1265.
- [31] K.S. Jones, S. Prussin and E.R. Weber, *J. Appl. Phys.* 62 (1987) p.4114 – 4117.
- [32] J. Liu, M.E. Law and K.S. Jones, *Solid-State Electron.* 38 (1995) p.1305–1312.
- [33] H.O.K. Kirchner, *Acta Metall.* 21 (1973) p.85 – 91.
- [34] J. Powell and J. Burke, *Philos. Mag.* 31 (1975) p.943–951.
- [35] B. Burton and M.V. Speight, *Philos. Mag. A* 53 (1986) p.385 – 402.
- [36] Y. Enomoto, *J. Phys-Condens. Mat.* 1 (1989) p.9785 – 9789.
- [37] D. Hull and D.J. Bacon *Introduction to Dislocations*, 4<sup>th</sup> edition Butterworth Heinemann, 2001.
- [38] J. Friedel *Dislocations*, Pergamon Press, Oxford, 1964.
- [39] J. Weertman, *Philos. Mag.* 11 (1965) p.1217–1223.
- [40] J. Lothe and J.P. Hirth, *J. Appl. Phys.* 38 (1967) p.845–848.
- [41] W.G. Wolfer, *J. Computer-Aided Mater. Des.* 14 (2007) p.403–417.
- [42] W. Cai, A. Arsenlis, C.R. Weinberger and V.V. Bulatov, *J. Mech. Phys. Solids* 54 (2006) p.561–587.
- [43] J.P. Hirth and J. Lothe *Theory of dislocations*, McGraw-Hill, New York, 1982.
- [44] A.Y. Kuksin, V.V. Stegailov and A.V. Yanilkin, *Doklady Phys.* 53 (2008) p.287–291.
- [45] A. Hikata, R.A. Johnson and C. Elbaum, *Phys. Rev. B* 2 (1970) p.4856–4863.
- [46] J.A. Gorman, D.S. Wood and T. Vreeland, *J. Appl. Phys.* 40 (1969) p.833–841.
- [47] D.L. Olmsted, L.G. Hector, W.A. Curtin and R.J. Clifton, *Modelling Simul. Mater. Sci. Eng.* 13 (2005) p.371.
- [48] S. Groh, E.B. Marin, M.F. Horstemeyer and H.M. Zbib, *Int. J. Plasticity* 25 (2009) p.1456 – 1473.
- [49] D. Rodney and G. Martin, *Phys. Rev. B* 61 (2000) p.8714–8725.
- [50] D. Caillard and J.L. Martin *Thermally activated mechanisms in crystal plasticity*, Pergamon, Amsterdam, 2003.
- [51] D.N. Seidman and R.W. Balluffi, *Philos. Mag.* 13 (1966) p.649 – 654.